


ORIGINAL ARTICLE

Released dsDNA-triggered inflammasomes serve as intestinal radioprotective targets

Long Chen^{1,2,1,a}, Ziwen Wang^{3,1,a}, Jie Wu^{1,1,a}, Quan Yao⁴, Jingjing Peng⁵, Chi Zhang¹, Hongdan Chen⁶, Yingjie Li¹, Zhongyong Jiang¹, Yunsheng Liu¹ & Chunmeng Shi¹ ¹State Key Laboratory of Trauma, Burns and Combined Injury, Institute of Rocket Force Medicine, Army Medical University, Chongqing, China²Shigatse Branch, Xinqiao Hospital, Army 953 Hospital, Army Medical University, Shigatse, China³Department of Cardiology, Geriatric Cardiovascular Disease Research and Treatment Center, 252 Hospital of PLA, Baoding, China⁴Integrative Cancer Center & Cancer Clinical Research Center, Sichuan Cancer Center, School of Medicine, Sichuan Cancer Hospital & Institute, University of Electronic Science and Technology of China, Chengdu, China⁵Department of Oncology, Western Theater General Hospital, Chengdu, China⁶Breast and Thyroid Surgical Department, Chongqing General Hospital, University of Chinese Academy of Sciences, Chongqing, China**Correspondence**C Shi, State Key Laboratory of Trauma, Burns and Combined Injury, Institute of Rocket Force Medicine, Army Medical University, Chongqing, China
E-mail: shicm@tmmu.edu.cn^aEqual contributors.

Received 21 October 2022;

Revised 5 May 2023;

Accepted 18 May 2023

doi: 10.1002/cti2.1452

Clinical & Translational Immunology
2023; 12: e1452**Abstract**

Objectives. Intestinal mucositis is the major side effect during abdominal or pelvic radiotherapy, but the underlying immunogen remains to be further characterised and few radioprotective agents are available. This study investigated the role of dsDNA-triggered inflammasomes in intestinal mucositis during radiotherapy. **Methods.** Pro-inflammatory cytokines were detected by ELISA. Radiation-induced intestinal injury in mice was analyzed by means of survival curves, body weight, HE staining of intestines, and intestinal barrier integrity. Western blot, immunofluorescence staining, co-immunoprecipitation assay and flow cytometry were used to investigate the regulatory role of dsDNA on inflammasomes. **Results.** Here, we show that a high level of IL-1 β and IL-18 is associated with diarrhoea in colorectal cancer (CRC) patients during radiotherapy, which accounts for intestinal radiotoxicity. Subsequently, we found that the dose-dependently released dsDNA from the intestinal epithelial cells (IECs) serves as the potential immunogenic molecule for radiation-induced intestinal mucositis. Our results further indicate that the released dsDNA transfers into the macrophages in an HMGB1/RAGE-dependent manner and then triggers absent in melanoma 2 (AIM2) inflammasome activation and the IL-1 β and IL-18 secretion. Finally, we show that the FDA-approved disulfiram (DSF), a newly identified inflammasome inhibitor, could mitigate intestinal radiotoxicity by controlling inflammasome. **Conclusion.** These findings indicate that the extracellular self-dsDNA released from the irradiated IECs is a potential immunogen to stimulate immune cells and trigger the subsequent intestinal mucositis, while blunting the dsDNA-triggered inflammasome in macrophages may represent an exciting therapeutic strategy for side effects control during abdominal radiotherapy.

Keywords: AIM2, DAMP, disulfiram, dsDNA, HMGB1, inflammasome, intestinal radiotoxicity

INTRODUCTION

Radiotherapy is an indispensable and effective therapy for abdominal cancers, such as colorectal cancer (CRC).^{1,2} Up to now, although radiotherapy strategies have been greatly improved,^{3,4} intestinal radiotoxicity like diarrhoea is still the major limiting factor during radiotherapy.^{5,6} Unfortunately, there are no available FDA-approved agents for intestinal radiotoxicity.

Studies on the death of intestinal epithelial cells (IECs) have greatly broadened the understanding of radiation-induced intestinal injury,^{7–10} but it is still challenging to control intestinal radiotoxicity by preventing IEC death, indicating the existence of potential uncovered mechanisms. There is growing evidence that extensive mucositis might be involved in intestinal radiotoxicity.^{11–19} Researchers have found that pro-inflammatory cytokines including IL-1 β and IL-18 greatly increase after radiation^{20–24} and serve as the important drivers of intestinal radiotoxicity.^{11,13,18} In addition, inflammasomes, the macromolecular complexes which trigger central and rapid inflammatory responses, and are accompanied by the secretion of mature IL-1 β and IL-18,²⁵ are recently reported to regulate radiation-induced tissue injury.^{10,26–28} However, the underlying immunogen in intestinal mucositis during radiotherapy is still not entirely clear, and further investigations are needed.

DNA, a classical damage-associated molecular pattern (DAMP), has been reported to trigger inflammasome activation and immunogenic response.^{26,29–31} Recently, two studies reported that radiation-induced DNA damage in the nuclei triggers AIM2 inflammasome-dependent pyroptosis in the epithelial cells,^{10,27} suggesting that DNA might serve as a potential immunogen for intestinal mucosa inflammation. As we know, inflammasomes are widely expressed in immune cells,²⁵ some studies reported that extracellular DNA could be captured by the phagocytes and trigger the pro-inflammatory response in autoimmune diseases.^{32–34} Researches have shown that the dsDNA could release from the irradiated tissues, but whether the extracellular dsDNA released from the IECs could stimulate phagocytes and trigger a broader pro-inflammatory response, then aggravate radiation-induced intestinal injury, remains to be elucidated.

This study indicates that extracellular self-dsDNA released from the irradiated IECs could transfer into the macrophages and trigger inflammasome activation and subsequent intestinal mucositis, broadening the understanding of intestinal mucositis during radiotherapy. Besides, our findings also suggest that blunting the dsDNA-triggered inflammasome-dependent IL-1 β and IL-18 secretion in the macrophages is an exciting therapeutic strategy for intestinal radiotoxicity, while the FDA-approved DSF is a promising candidate drug for inflammasome control during abdominal radiotherapy.

RESULTS

IL-1 β and IL-18 secretion account for intestinal radiotoxicity

To investigate whether intestinal radiotoxicity is associated with the pro-inflammatory cytokines, IL-1 β and IL-18 levels were first detected in the peripheral blood of CRC patients before and 48 h after radiotherapy. Our results showed that 35 patients exhibited various degrees of diarrhoea after radiotherapy (Figure 1a). Besides, a significant increase in IL-1 β (Figure 1b) and IL-18 (Supplementary figure 1a) was detected in the peripheral blood after radiotherapy, and we also observed that patients with higher-grade diarrhoea showed higher levels of IL-1 β and IL-18 (Figure 1c and Supplementary figure 1b). To further investigate the correlation between pro-inflammatory cytokines and intestinal radiotoxicity, the mice were exposed to whole abdominal radiation (WAI; Figure 1d), and then the IL-1 β and IL-18 levels in the peritoneal lavage fluid were analysed 48 h after WAI. Our data showed that WAI induced a dose-dependent release of IL-1 β and IL-18 in mice (Figure 1e and Supplementary figure 1c). Similarly, the release of IL-1 β and IL-18 was positively correlated with the severity of diarrhoea (Figure 1f and Supplementary figure 1d). In addition, serum FITC-dextran, which reflects the destruction of intestinal epithelial barrier integrity, also had a positive correlation with IL-1 β and IL-18 levels in the PLF (Figure 1g and Supplementary figure 1e), further

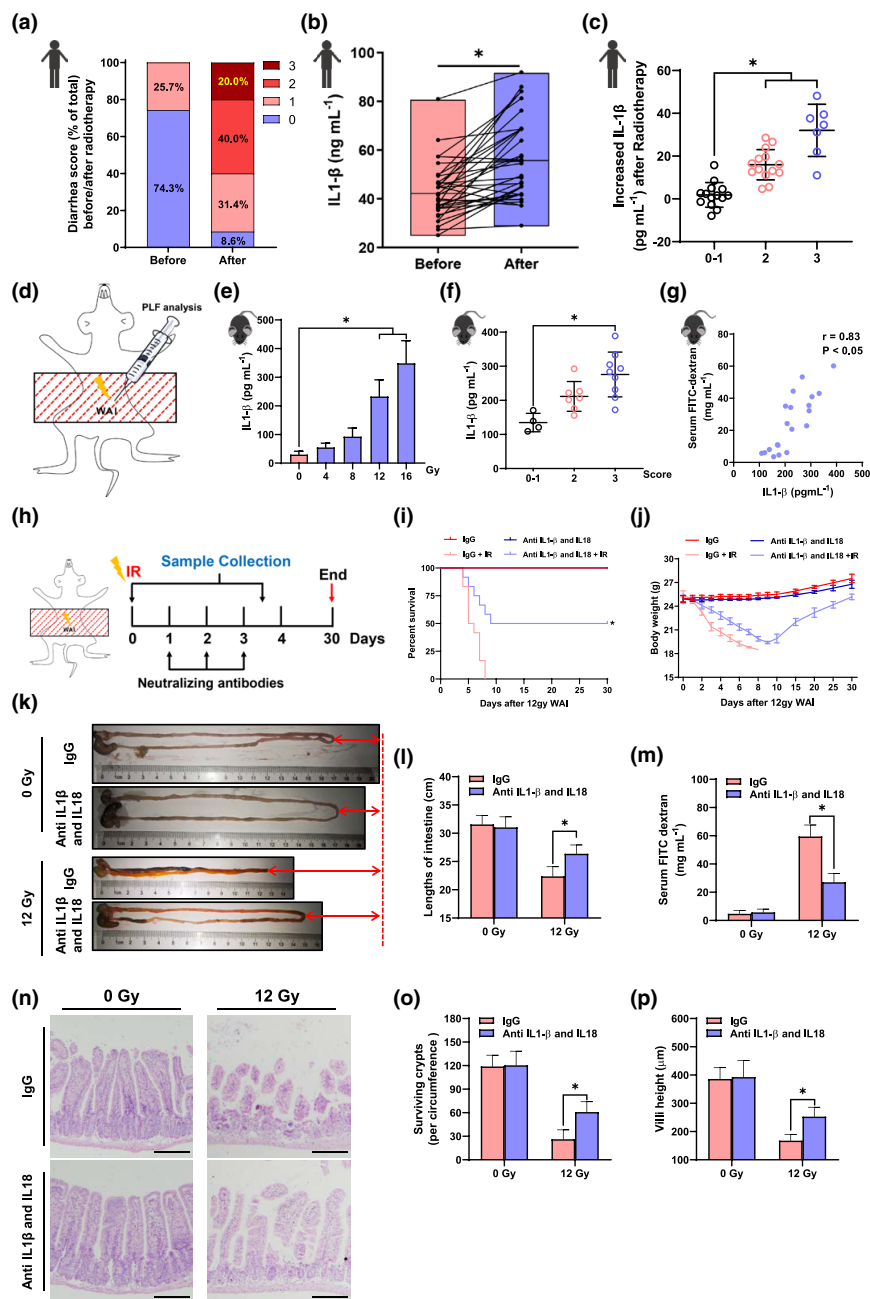


Figure 1. Inflammation-related pro-inflammatory cytokines contribute to intestinal radiotoxicity. **(a)** The percentage of different grades of diarrhoea among 35 patients with abdominal radiotherapy. **(b)** Serum IL-1 β in the patients before and 48 h after abdominal radiotherapy. **(c)** Increased serum IL-1 β level in patients with different grades of diarrhoea. **(d)** Schematic diagram of WAI in mice, and the PLF was analysed 48 h after WAI. **(e)** IL-1 β level in the PLF of mice 48 h after exposure to different doses of WAI. $n = 5$. **(f)** IL-1 β level in the PLF of mice with different grades of diarrhoea. **(g)** The Pearson correlation analysis between the PLF IL-1 β level and the serum FITC-dextran level; the higher serum FITC-dextran level reflects more severely disrupted intestinal barrier integrity. **(h)** Schematic diagram of 12 Gy WAI, sample collection and treatment in mice. Neutralising antibodies, 1 mg mouse⁻¹, intraperitoneally. Survival curves **(i)** and body weight over time **(j)** of mice treated with neutralising antibodies or IgG after 12 Gy WAI. $n = 5$. Photographs **(k)** and statistical analysis **(l)** of the intestine length of mice 3.5 days after WAI. **(m)** The serum FITC-dextran level in mice 3.5 days after WAI. **(n)** H&E-stained sections of the mice intestine 3.5 days after WAI. Scale bars: 100 μ m. Statistical analysis of surviving crypts **(o)** and villi height **(p)** per section 3.5 days after WAI. $n = 5$. For **b**, **c**, **f** and **g**, every point indicates an individual patient or mouse. For **b**, statistical significance was analysed by the paired two-tailed t -test was used. For **c**, **e** and **f**, statistical significance was analysed by one-way ANOVA (Dunnett). For **i**, Kaplan–Meier survival analysis. For **l–p**, $n = 5$, statistical significance was analysed by two-way ANOVA (Bonferroni). * $P < 0.05$. Error bar, means \pm SD.

suggesting that IL-1 β and IL-18 secretion might be associated with intestinal radiotoxicity.

To investigate whether IL-1 β and IL-18 secretion contributes to radiation-induced intestinal injury, mice were exposed to 12 Gy WAI, and treated with neutralising antibodies of IL-1 β and IL-18 as described in Figure 1h. Our results showed that the neutralising antibodies protected mice from radiation-induced mortality (Figure 1i) and bodyweight loss (Figure 1j). To further evaluate the radioprotective effects of IL-1 β and IL-18 blockade, mice were sacrificed and pathological examination was performed 3.5 days after WAI. Our data showed that neutralising antibodies treatment reduced the radiation-induced shortening of the small intestine (Figure 1k and l) and the destruction of intestinal barrier integrity (the higher serum FITC-dextran level reflects more severely disrupted intestinal barrier integrity; Figure 1m). Besides, the results of HE staining showed that the crypt-villus architecture and survival crypts were also well protected in the mice with neutralising antibodies treatment (Figure 1n–p). These results indicate that IL-1 β and IL-18 secretion contributes to intestinal radiotoxicity.

Self-dsDNA release is associated with IL-1 β and IL-18 secretion and intestinal radiotoxicity

Gut microbiota plays an important role in inflammasome activation and has been reported to regulate intestinal radiotoxicity.^{11,35–39} To investigate whether radiation-induced inflammasome activation is related to the microbiota, the gut microbiota was deleted using a combination of antibiotics (Supplementary figure 2a) in mice. Unexpectedly, the IL-1 β and IL-18 secretion was still detected in the PLF (Supplementary figure 2b and c), suggesting that the host-derived immunogens might be involved in the radiation-induced IL-1 β and IL-18 secretion.

Previous studies showed that radiation induces self-dsDNA release from the irradiated tissues,⁴⁰ which might be a potential immunogen for stimulating inflammasome-dependent IL-1 β and IL-18 secretion. To verify this hypothesis, we first analysed the dsDNA level in the peripheral blood from CRC radiotherapy patients. Similar to the results of IL-1 β and IL-18, dsDNA increased significantly after radiotherapy (Figure 2a) and higher dsDNA level were detected in the patients

with higher-grade diarrhoea (Figure 2b). More importantly, the increased dsDNA had a positive correlation with the release of IL-1 β and IL-18 (Figure 2c and d). Then, we analysed the dsDNA in the PLF from mice after WAI (Figure 2e). Like the IL-1 β and IL-18, radiation induced a dose-dependent release of dsDNA in the PLF; more dsDNA was also detected in the mice with higher-grade diarrhoea (Figure 2g), and dsDNA level had a positive correlation with the destruction of intestinal epithelial barrier integrity (Figure 2h). In addition, our results showed that the dsDNA was still detected in PLF from the microbiota-deleted mice (Supplementary figure 2d), suggesting that the released dsDNA in the PLF might derive from the host but not the microbiota. Further analysis confirmed this hypothesis by comparison with the spleen DNA and the faeces DNA (Supplementary figure 2e). These results suggest that higher release of host-derived dsDNA release might be associated with IL-1 β and IL-18 secretion after radiotherapy.

To further verify the role of dsDNA in the IL-1 β and IL-18 secretion and intestinal radiotoxicity, mice were exposed to WAI and treated with DNase (Figure 2i). Our results showed that DNase treatment significantly decreased the dsDNA level (Supplementary figure 2f), and the secretion of IL-1 β and IL-18 (Figure 2j and k) in the PLF after WAI. In addition, DNase treatment effectively mitigates radiation-induced mortality (Figure 2l) and bodyweight loss (Figure 2m), destruction of intestinal epithelial barrier integrity (Figure 2n), and intestinal tissue injury (Figure 2o–q). These results indicate that radiation-induced self-dsDNA release contributes to intestinal mucositis.

IEC-derived dsDNA triggers inflammasome in macrophages

Then, we further explore the underlying mechanisms of dsDNA in IL-1 β and IL-18 secretion. To investigate whether radiation could induce dsDNA release *in vitro*, the HCT116 cell line was used as an intestinal epithelial cell model *in vitro*.^{26,41,42} Our results showed that radiation induced a dose-dependent release of dsDNA in the culture supernatants (Figure 3a). Then, we cocultured the HCT116 cells with the bone marrow-derived macrophages (BMMs) to investigate whether the dsDNA released from HCT116 cells could transfer into the BMMs. First, the HCT116 cells were prelabelled with the DNA-

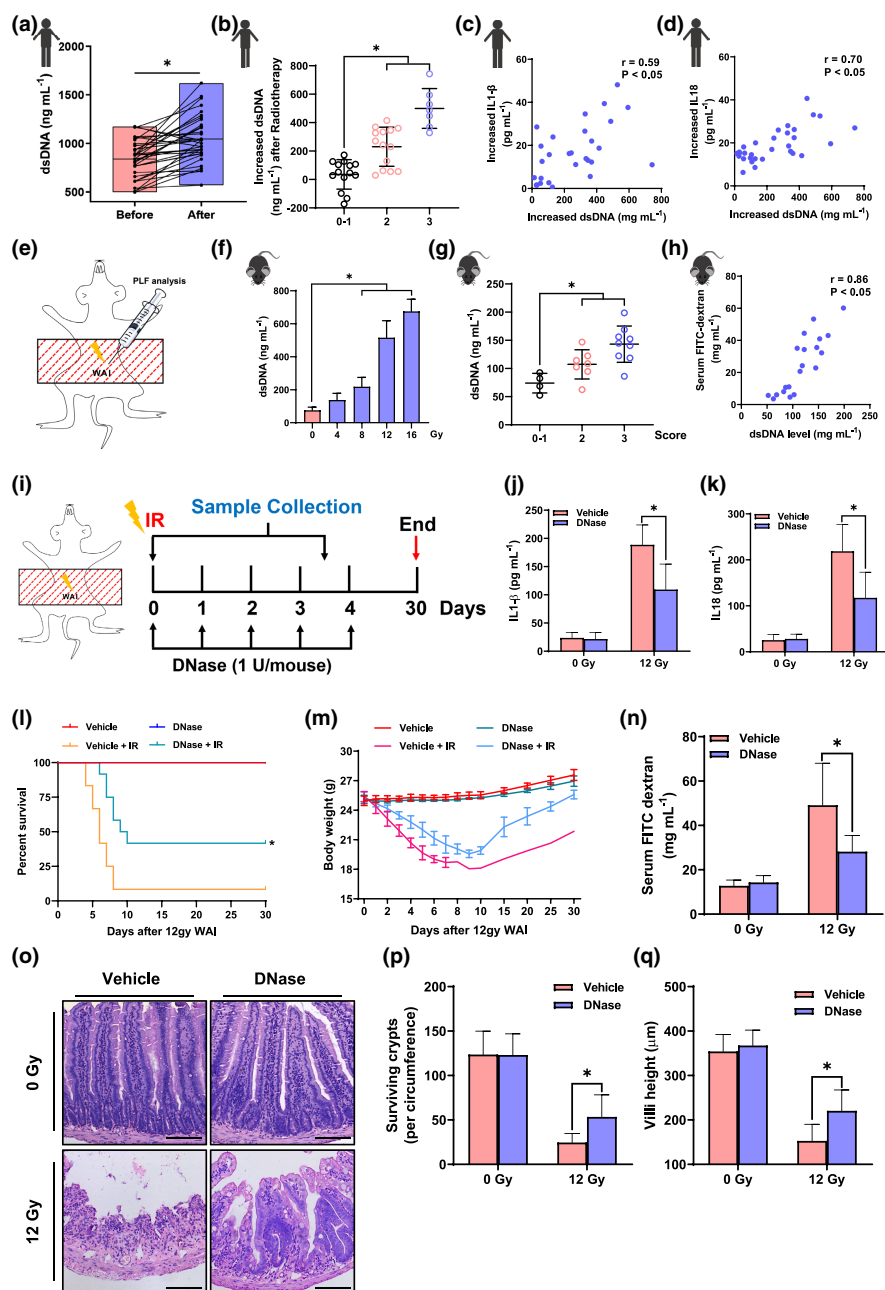


Figure 2. Self-dsDNA release is associated with inflammasome-related pro-inflammatory cytokines secretion and intestinal radiotoxicity. **(a)** Serum dsDNA level in the patients before and 48 h after abdominal radiotherapy. **(b)** Increased serum dsDNA level in patients with different grades of diarrhoea. **(c)** The Pearson correlation analysis between the increased serum dsDNA level and the increased serum IL-1 β level. **(d)** The Pearson correlation analysis between the increased serum dsDNA level and the increased serum IL-18 level. **(e)** Schematic diagram of WAI in mice, and the PLF was analysed 48 h after WAI. **(f)** dsDNA level in the PLF of mice exposed to different doses of WAI. $n = 5$. **(g)** The dsDNA level in the PLF of mice with different grades of diarrhoea. **(h)** The Pearson correlation analysis between the PLF dsDNA level and the serum FITC-dextran level. **(i)** Schematic diagram of 12 Gy WAI, sample collection and treatment in mice. The PLF IL-1 β **(j)** and IL-18 **(k)** level 48 h after 12 Gy WAI. $n = 5$. Survival curves **(l)** and bodyweight over time **(m)** of mice treated with DNase or vehicle after 12 Gy WAI. $n = 12$. **(n)** The serum FITC-dextran level in mice 3.5 days after WAI. $n = 12$. **(o)** H&E-stained sections of the mice intestine 3.5 days after WAI. Scale bars: 100 μm . Statistical analysis of surviving crypts **(p)** and villi height **(q)** per section 3.5 days after WAI. $n = 5$. For **a**, **c**, **d**, **g** and **h**, every point indicates an individual patient or mouse. For **a**, statistical significance was analysed by the paired two-tailed t -test. For **b**, **f** and **g**, statistical significance was analysed by one-way ANOVA (Dunnett). For **l**, Kaplan–Meier survival analysis. For **n–q**, $n = 5$, statistical significance was analysed by two-way ANOVA (Bonferroni). $*P < 0.05$. Error bar, means \pm SD. Data are shown from one representative experiment, based on at least three experiments, which produced similar results.

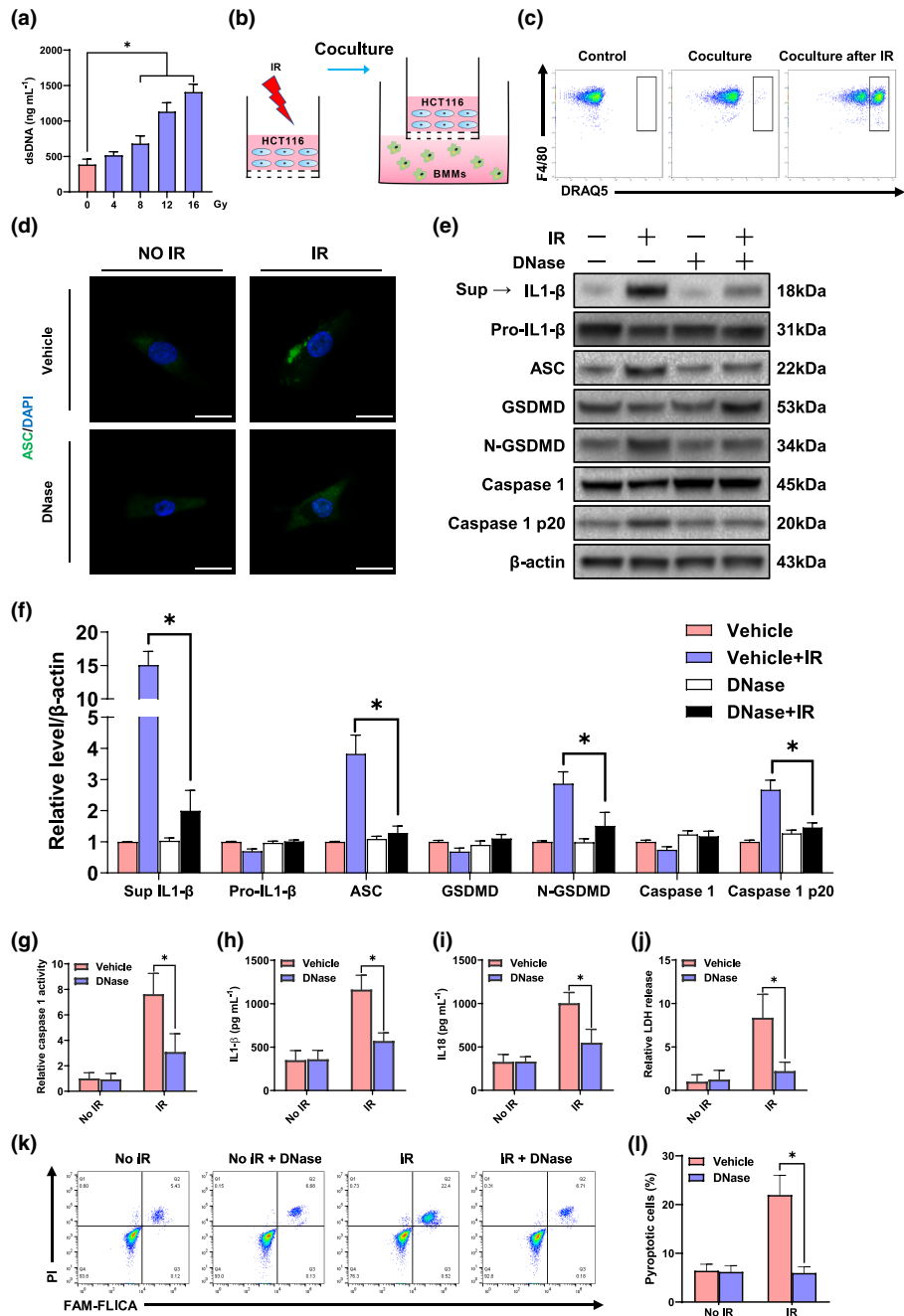


Figure 3. dsDNA released from the intestinal epithelial cells triggers inflammasome activation in macrophages. **(a)** The dsDNA level in the culture supernatants of HCT116 cells was detected 48 h after different doses of radiation. $n = 5$. **(b)** Schematic diagram of the coculture system of HCT116 cells and BMMs. HCT116 cells were exposed to 12 Gy radiation and then cocultured with the BMMs using a 0.4- μ m Transwell plate. **(c)** dsDNA in the irradiated HCT116 cells was prestained using DRAQ5 (10 μ M) and then cocultured with BMMs for 24 h, then the BMMs were collected and analysed using flow cytometry. F4/80, the marker of BMMs. **(d)** The ASC aggregates in the BMMs were analysed via confocal microscopy. ASC, green; nuclei, DAPI. Scale bars: 10 μ m. **(e)** IL-1 β in the Sup and Pro-IL-1 β , ASC, GSDMD, N-GSDMD, Caspase-1, and Caspase-1 p20 from the BMMs lysate in the coculture system were detected by Western blot. Sup, coculture supernatants. **(f)** Western blot quantification. $n = 3$. **(g)** Relative caspase 1 activity in the cell extract of BMMs. $n = 5$. The IL-1 β **(h)**, IL-18 **(i)** and LDH **(j)** levels in the coculture supernatants. $n = 5$. Pyroptosis was detected **(k)** and statistically analysed **(l)** by flow cytometry. Pyroptotic cells are cells with double positivity of Caspase-1 and PI. $n = 3$. For **d–k**, DNase (0.005 U mL⁻¹) was added to the coculture media, and BMMs were analysed 48 h after coculture. For **a**, statistical significance was analysed by one-way ANOVA (Dunnett). For **f–k**, statistical significance was analysed by two-way ANOVA (Bonferroni). * $P < 0.05$. Error bar, means \pm SD.

intercalating dye DRAQ5 and then exposed to radiation or not, followed by coculture with BMMs (Figure 3b). Our results showed that a minor population of BMMs were positive for HCT116-derived DRAQ5 after coculture, while radiation significantly increased the positive rate when compared to the control group (without coculture; Figure 3c), suggesting that radiation promoted the transfer of HCT116-derived dsDNA into the BMMs. Next, we aimed to investigate whether the released dsDNA could trigger the inflammasome in BMMs. Immunofluorescence staining showed that ASC, a key adaptor of inflammasomes, formed obvious aggregates in BMMs after coculture with the irradiated HCT116 cells, while DNase treatment abolished the aggregated ASC (Figure 3d). Besides, the released dsDNA also triggered downstream consequences of inflammasome including the cleaved Caspase 1 and GSDMD (Figure 3e–g), the secretion of IL-1 β (Figure 3e, f and h), IL-18 (Figure 3i), the release of lactate dehydrogenase (LDH; Figure 3j) and the pyroptosis (Figure 3k and l). These results showed that radiation-induced IEC-derived dsDNA could transfer into macrophages and contribute to inflammasome activation.

IEC-derived dsDNA triggers inflammasome in macrophages through the HMGB1-RAGE axis

To further validate how the dsDNA transfers into BMMs, the dsDNA in the culture supernatants of irradiated HCT116 cells was purified and then added to the culture media of BMMs. Unexpectedly, the purified dsDNA alone without Lipo could not trigger inflammasome BMMs (Supplementary figure 3a–i), while the purified dsDNA effectively triggered inflammasome and the related downstream consequences in BMMs upon the addition of DNA transfection reagent (Lipo, a DNA transfection reagent), indicating that it is difficult for the purified dsDNA to transfer into macrophages alone. Thus, some other substances could be involved in the transfer of dsDNA into macrophages. Of note, HMGB1, a multifunctional nuclear DNA-binding protein, has been widely reported to release after radiation.⁴³ A recent study shows that extracellular HMGB1 facilitates macrophage activation in lupus nephritis by promoting the intracellular accumulation of self-dsDNA.³² To investigate whether HMGB1 contributes to the dsDNA-triggered inflammasome

activation, we first analysed the HMGB1 level after radiation. Our results showed that HMGB1 significantly increased in the peripheral blood from CRC radiotherapy patients (Figure 4a), and a higher HMGB1 level was detected in the patients with higher-grade diarrhoea (Figure 4b). Besides, radiation induced a dose-dependent release of HMGB1 in the PLF of mice after WAI and in the irradiated HCT116 culture supernatants (Figure 4c and d). To investigate whether HMGB1 promotes the transfer of dsDNA into macrophages, the purified dsDNA and recombinant HMGB1 (rHMGB1) were simultaneously added to the culture media of BMMs. Our results showed that rHMGB1 reverted the inflammasome-triggered capacity of the purified dsDNA in the BMMs (Figure 4e–m). These results suggest that HMGB1 is an important participant in the dsDNA-triggered inflammasome activation.

Studies have shown that the receptor for RAGE is a classical HMGB1 recognising receptor, which is involved in intracellular internalisation of the HMGB1-DNA complex.³² To further investigate whether the HMGB1/RAGE axis is involved in the dsDNA transfer, specific HMGB1 inhibitor glycyrrhizin and the specific RAGE inhibitor FPS-ZM1 were used in the coculture system of HCT116 and BMMs. As predicted, both glycyrrhizin and FPS-ZM1 significantly decreased the dsDNA transfer into the BMMs (Figure 5a) and blunted the dsDNA-triggered inflammasome activation and the downstream consequences (Figure 5b–j). To further validate the importance of HMGB1 *in vivo*, mice were treated with glycyrrhizin after WAI. Our results confirmed that inhibiting HMGB1 using glycyrrhizin could effectively blunt the inflammasome-dependent secretion of IL-1 β and IL-18 (Figure 5k and l) *in vivo*, while there was no obvious effect on the dsDNA level (Figure 5m). In addition, glycyrrhizin mitigated the radiation-induced mortality (Figure 5n) and bodyweight loss (Figure 5o), destruction of intestinal epithelial barrier integrity (Figure 5p), and intestinal tissue injury (Figure 5q–s). These results suggest that dsDNA triggers inflammasome in macrophages through the HMGB1-RAGE axis.

AIM2 accounts for the dsDNA-triggered inflammasome

AIM2 and Nod-like receptor protein 3 (NLRP3) are two known DNA sensors for inflammasome formation by recruiting the apoptosis-associated speck-like proteins containing a CARD

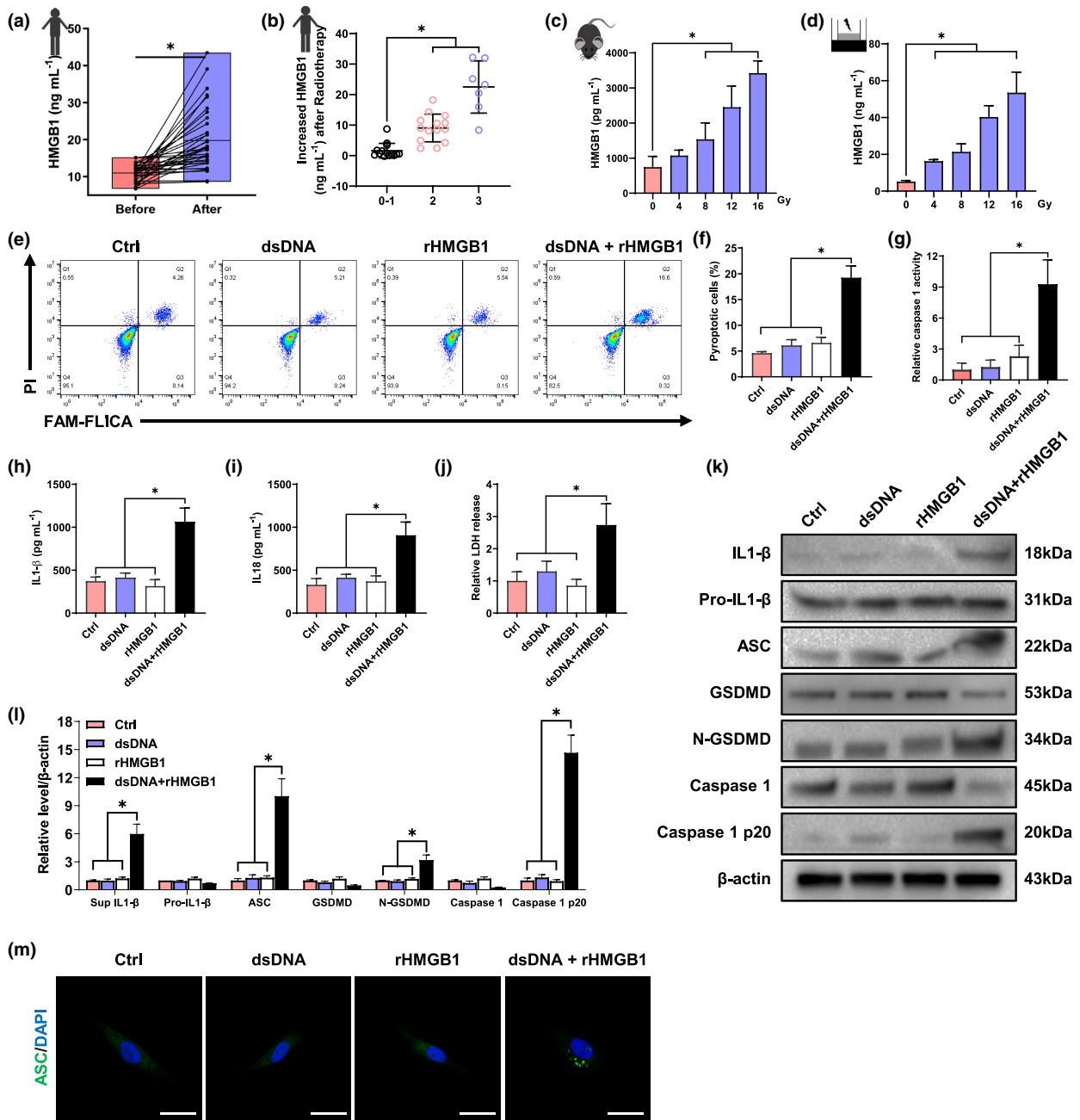


Figure 4. HMGB1 is required for dsDNA-triggered inflammasome activation in macrophages. **(a)** Serum HMGB1 level in the patients before and 48 h after abdominal radiotherapy. **(b)** Increased serum HMGB1 level in patients with different grades of diarrhoea. **(c)** The HMGB1 level in the PLF of mice exposed to different doses of WAI. $n = 5$. **(d)** The HMGB1 level in the culture supernatants of HCT116 cells was detected 48 h after different doses of radiation. $n = 5$. Pyroptosis was detected **(e)** and statistically analysed **(f)** by flow cytometry. **(g)** Relative caspase 1 activity in the cell extract of BMMs. $n = 5$. The IL-1 β **(h)**, IL-18 **(i)** and LDH **(j)** levels in the coculture supernatants. $n = 5$. **(k)** IL-1 β in the Sup and Pro-IL-1 β , ASC, GSDMD, N-GSDMD, Caspase-1, Caspase-1 p20 from the BMMs lysate in the coculture system were detected by Western blot. Sup, coculture supernatants. **(l)** Western blot quantification. $n = 3$. **(m)** The ASC aggregates in the BMMs were analysed via confocal microscopy. ASC, green; nuclei, DAPI. Scale bars: 10 μ m. For **a–h**, purified dsDNA (0.5 μ g mL⁻¹) from the culture supernatants of irradiated HCT116 cells was added to the BMMs media with or without Lipo for 48 h. Lipo, a DNA transfection reagent. For **m–t**, purified dsDNA (0.5 μ g mL⁻¹) from the culture supernatants of irradiated HCT116 cells was added to the BMMs media with or without rHMGB1 (50 ng mL⁻¹) for 48 h. For **a**, statistical significance was analysed by the paired two-tailed t -test. For **b–l**, statistical significance was analysed by one-way ANOVA (Dunnett). For **a** and **b**, every point indicates an individual patient. * $P < 0.05$. Error bar, means \pm SD.

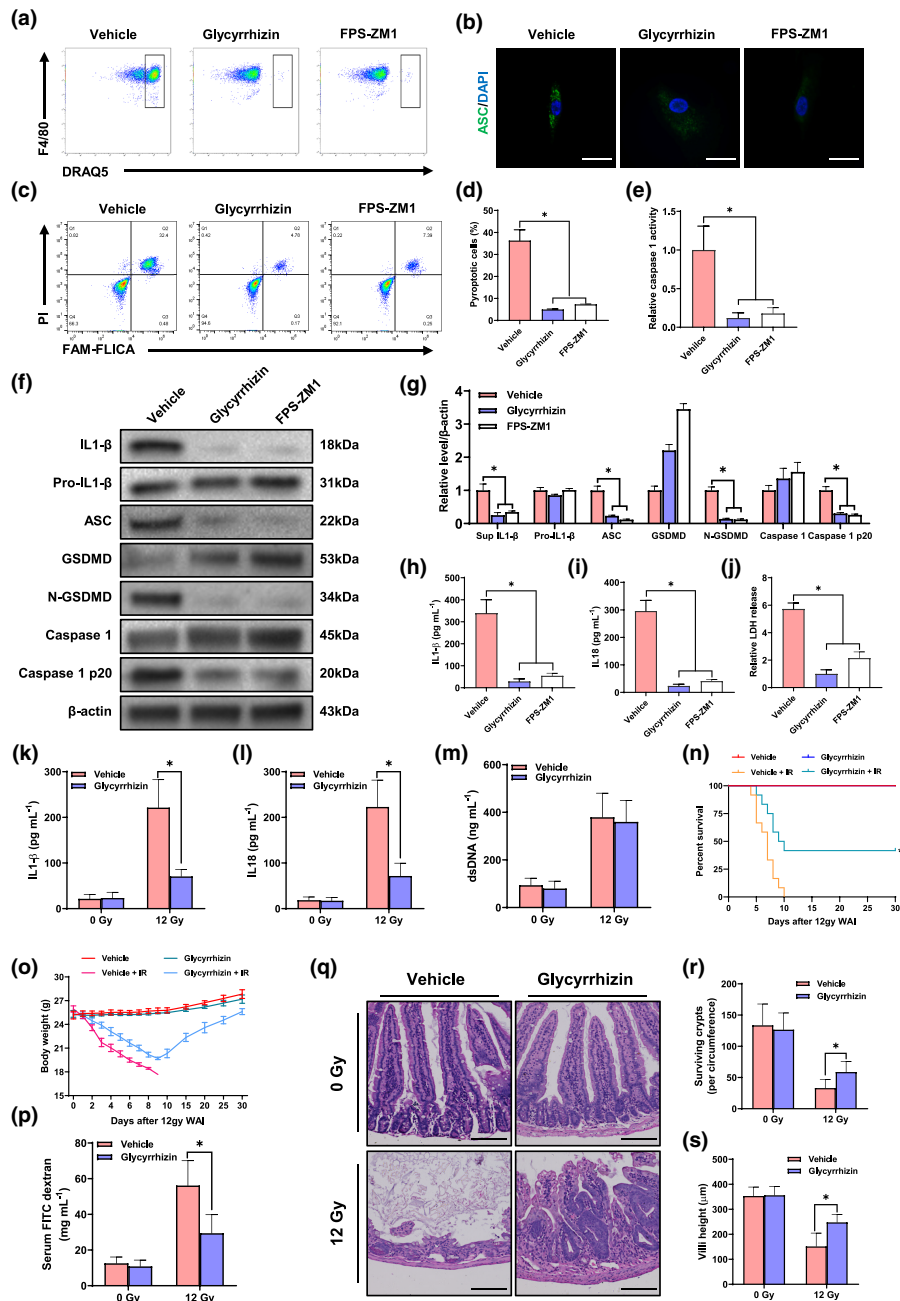


Figure 5. dsDNA triggers inflammasome activation through the HMGB1-RAGE axis. **(a)** dsDNA in the irradiated HCT116 cells was prestained using DRAQ5 (10 μ M) and then cocultured with BMMs for 24 h, then the BMMs were collected and analysed using flow cytometry. F4/80, the marker of BMMs. **(b)** The ASC aggregates in the BMMs were analysed via confocal microscopy. ASC, green; nuclei, DAPI. Scale bars: 10 μ m. Pyroptosis was detected **(c)** and statistically analysed **(d)** by flow cytometry. Pyroptotic cells are cells with double positivity of Caspase-1 and PI. $n = 3$. **(e)** Relative caspase 1 activity in the cell extract of BMMs. $n = 5$. **(f)** IL-1 β in the Sup and Pro-IL-1 β , ASC, GSDMD, N-GSDMD, Caspase-1, Caspase-1 p20 from the BMMs lysate in the coculture system were detected by Western blot. Sup, coculture supernatants. **(g)** Western blot quantification. The IL-1 β **(h)**, IL-18 **(i)** and LDH **(j)** levels in the coculture supernatants. $n = 5$. The PLF IL-1 β **(k)**, IL-18 **(l)** and dsDNA **(m)** level 48 h after 12 Gy WAI. $n = 5$. Survival curves **(n)** and body weight over time **(o)** of mice treated with DNase or vehicle after 12 Gy WAI. $n = 12$. **(p)** The serum FITC-dextran level in mice 3.5 days after WAI. **(q)** H&E-stained sections of the mice intestine 3.5 days after WAI. Scale bars: 100 μ m. Statistical analysis of surviving crypts **(r)** and villi height **(s)** per section 3.5 days after WAI. $n = 5$. For **b–i**, glycyrrhizin (1 mM), FPS-ZM1 (500 nM) or vehicle was added in the coculture media, and BMMs were analysed 48 h after coculture. For **d–j**, statistical significance was analysed by one-way ANOVA (Dunnett). For **k–s**, statistical significance was analysed by two-way ANOVA (Bonferroni). * $P < 0.05$. Error bar, means \pm SD. Data are shown from one representative experiment, based on at least three experiments, which produced similar results.

(ASC).^{10,26,31,33,44–48} Then, we further investigated the specific type of dsDNA-triggered inflammasome. Our results showed that no obvious aggregates of NLRP3-ASC complexes were observed in the BMMs when coculturing with the irradiated HCT116 cells, while the NLRP3-positive inductor LPS induced observable colocalization of aggregated NLRP3 and ASC (Figure 6a) in the BMMs. In addition, MCC950,⁴⁹ an NLRP3 inflammasome inhibitor, also did not reverse the dsDNA-triggered inflammasome activation and the downstream consequences (Supplementary figure 4a–h). Conversely, obvious AIM2 aggregates were colocalised with ASC in the BMMs when coculturing with the irradiated HCT116 cells (Figure 6b). To further validate the AIM2-ASC interaction, co-immunoprecipitation (CoIP) of AIM2 and ASC was performed. Our results showed that dsDNA significantly promoted the interaction between AIM2 and ASC (Figure 6c), suggesting that dsDNA-triggered inflammasome activation might be related to AIM2. To further test this hypothesis, AIM2 siRNA was used to knock down the AIM2 expression level (Figure 6d and f). As expected, AIM2 knockdown significantly blunts the dsDNA-triggered inflammasome activation and the downstream consequences (Figure 6e and g–m) in the BMMs cocultured with the irradiated HCT116 cells. These results showed that IEC-derived dsDNA mainly triggers AIM2 but not NLRP3-dependent inflammasome in macrophages.

The FDA-approved DSF ameliorates intestinal radiotoxicity

As indicated above, dsDNA-triggered AIM2 inflammasome contributes to intestinal radiotoxicity. However, up to now, there are no specific AIM2-inflammasome inhibitors. Thus, we aimed to further investigate the protective effects on intestinal radiotoxicity by targeting the AIM2-inflammasome downstream consequences using four inhibitors, including thalidomide (THA),²⁶ VX765,⁵⁰ and the FDA-approved DSF⁵¹ and dimethyl fumarate (DMF)⁵² as shown in Figure 7a and b. As expected, mice treated with the four promising agents were protected from radiation-induced mortality (Figure 7c), bodyweight loss (Figure 7d), diarrhoea (Figure 7e), destruction of intestinal barrier integrity (Figure 7f), and intestinal tissue injury (Figure 7g–k). These results indicated that

blunting the AIM2 inflammasome could mitigate intestinal radiotoxicity.

To further evaluate the possibility of clinical application, we study the radioprotective effects on tumors.⁴ The inexpensive and tolerable DSF, the FDA-approved agent for alcoholism treatment, has shown potential antitumor activity.^{53–56} Besides, a recent study identified that DSF could specifically inhibit inflammasome-dependent secretion of IL-1 β and IL-18 by blocking GSDMD pore formation (Figure 7a).⁵¹ To further investigate whether DSF reduces the antitumor efficiency during radiotherapy, MC38 xenograft model and fractionated radiotherapy were performed (Figure 8a). Consistent with the previous reports,^{53–56} DSF exhibited potential antitumor effects (Figure 8b–d). Unexpectedly, the combinational therapy of DSF and radiotherapy possessed enhanced antitumor effects than radiotherapy or DSF only (Figure 8b–d). More importantly, DSF mitigated intestinal radiotoxicity, including diarrheal score (Figure 8e), bodyweight loss (Figure 8f), shortening of the small intestine (Figure 8g and h), reduction of intestinal barrier integrity (Figure 8i), inflammasome-dependent cytokines secretion (Figure 8j and k) and destruction of crypt-villus architecture (Figure 8l–n). These results suggest that DSF is a potential candidate drug for mitigating intestinal radiotoxicity and simultaneously does not affect the antitumor effect during radiotherapy.

DISCUSSION

Up to now, there are no available treatments for intestinal radiotoxicity,⁴ which could be related to complicated mechanisms. Over the years, researchers have revealed multiple types of cell death in the IEC loss after radiation^{7–10} and attempted to rescue the radiation-induced IEC death, but intestinal radiotoxicity remains refractory. Recently, some studies focussed on the secondary inflammatory response after IEC death and suggested that extensive mucositis accounts for intestinal radiotoxicity.^{11,17–19} Pieces of evidence show that pro-inflammatory cytokines including IL-1 β and IL-18 are greatly released in radiation-induced inflammation,²⁴ suggesting they might play an important role in intestinal radiotoxicity.^{11,13,18} Here, our results indicate that a higher level of IL-1 β and IL-18 is associated with diarrhoea in CRC patients during radiotherapy. Besides, radiation induces a dose-dependent

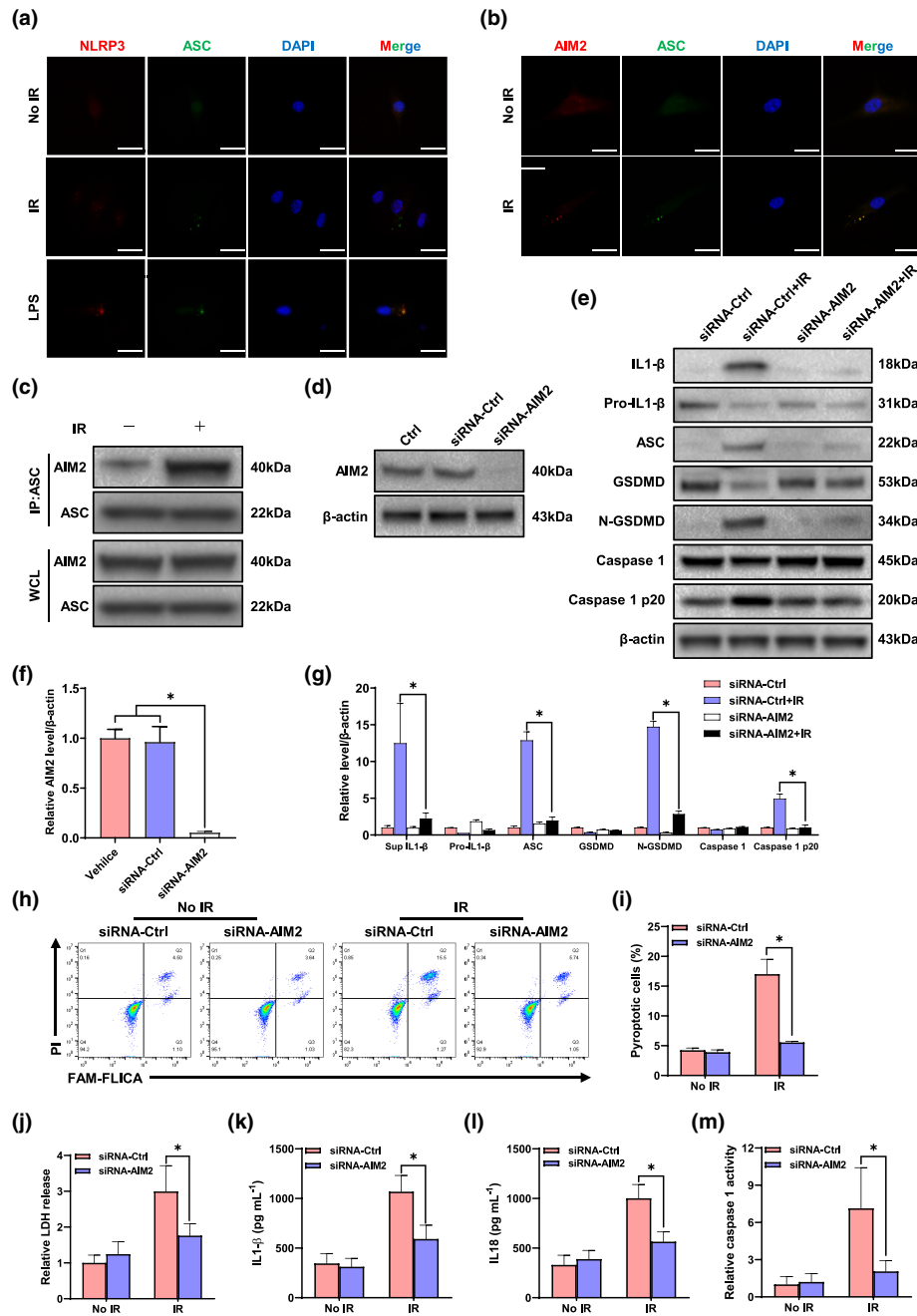


Figure 6. AIM2 accounts for the dsDNA-triggered inflammasome activation in macrophages. **(a)** The subcellular localisation of ASC (green) and NLRP3 (red) was analysed via confocal microscopy. nuclei, DAPI. Scale bars: 10 μ m. **(b)** The subcellular localisation of ASC (green) and AIM2 (red) was analysed via confocal microscopy. nuclei, DAPI. Scale bars: 10 μ m. LPS, the NLRP3 positive inducer used as a positive control. **(c)** The interaction of ASC and AIM2 in BMMs was co-immunoprecipitated and detected by western blotting (top). The whole-cell lysates of BMMs were analysed by Western blot (bottom). **(d)** The knockdown efficiency of AIM2 siRNA in BMMs was detected by Western blot. **(e)** IL-1 β in the Sup and Pro-IL-1 β , ASC, GSDMD, N-GSDMD, Caspase-1, Caspase-1 p20 from the BMMs lysate in the coculture system were detected by Western blot. Sup, coculture supernatants. **(f)** Western blot quantification of **d**. $n = 3$. **(g)** Western blot quantification of **e**. $n = 3$. Pyroptotic cells were detected **(h)** and statistically analysed **(i)** by flow cytometry. Pyroptotic cells are cells with double positivity of Caspase-1 and PI. $n = 3$. The LDH **(j)**, IL-1 β **(k)** and IL-18 **(l)** levels in the coculture supernatants. $n = 5$. **(m)** Relative caspase 1 activity in the cell extract of BMMs. $n = 5$. For **a–k**, BMMs or the coculture supernatants were analysed 48 h after coculture with the irradiated HCT116 cells. For **d–k**, BMMs were pretreated with siRNA-AIM2 or siRNA-Ctrl 48 h before coculture. For **f**, statistical significance was analysed by one-way ANOVA (Dunnett). For **g–m**, statistical significance was analysed by two-way ANOVA (Bonferroni). * $P < 0.05$. Error bar, means \pm SD.

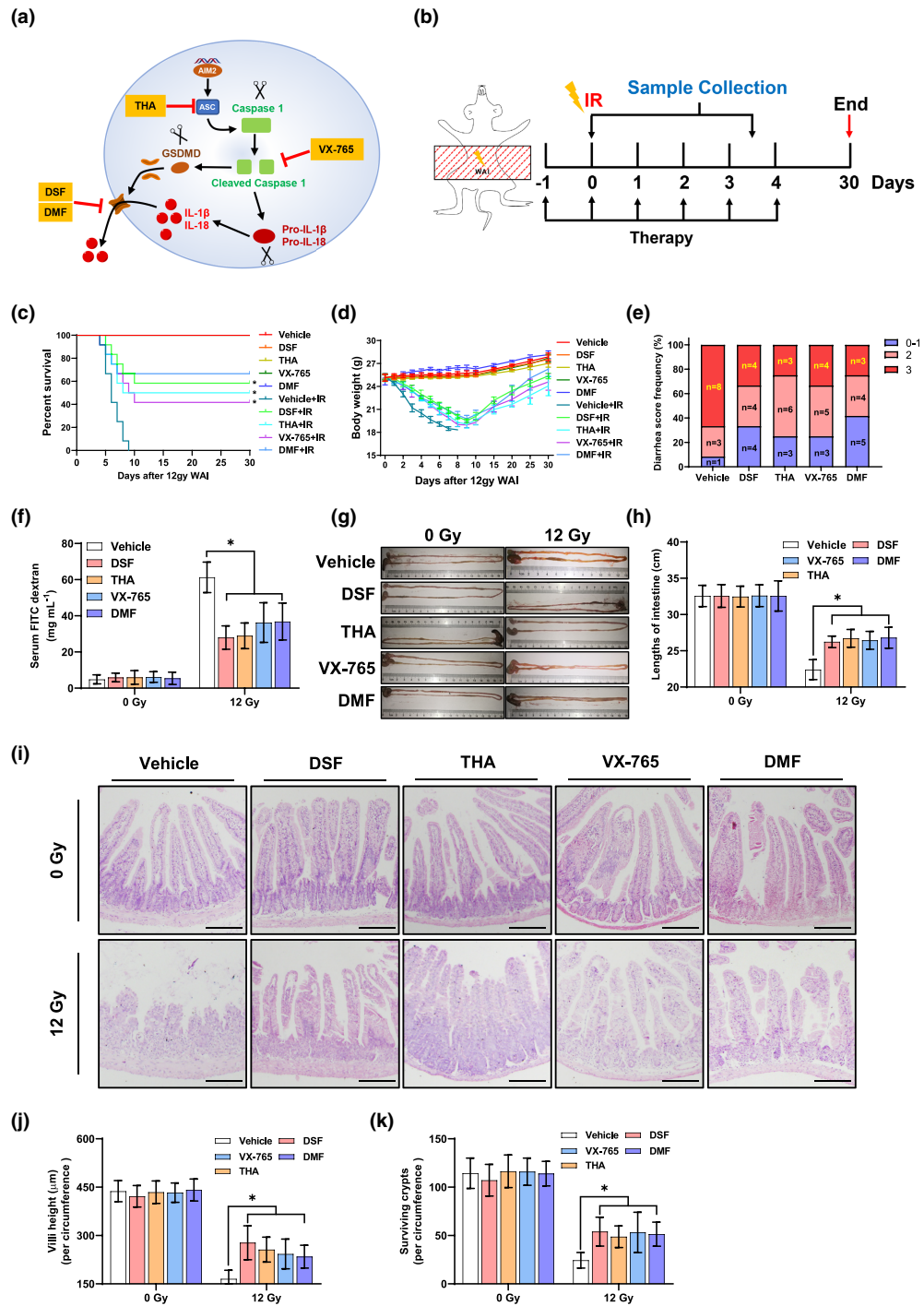


Figure 7. Blunting the inflammasome ameliorates intestinal radiotoxicity. **(a)** Cellular map of AIM2 inflammasome and the downstream consequences targeted by pharmacological agents. **(b)** Schematic diagram of 12 Gy WAI, sample collection and treatment in mice. Survival curves **(c)** and body weight over time **(d)** of mice treated with indicated agents or vehicles after WAI. $n = 12$. **(e)** The percentage of different grades of diarrhoea among mice treated with indicated agents after WAI. No obvious diarrhoea was observed in mice that were not exposed to WAI. **(f)** The serum FITC-dextran level in mice was detected 3.5 days after WAI. Photographs **(g)** and statistical analysis **(h)** of the intestine length of mice 3.5 days after WAI. **(i)** H&E-stained sections of the mice intestine 3.5 days after WAI. Scale bars: 100 μ m. Statistical analysis of villi height **(j)** and surviving crypts **(k)** per section 3.5 days after WAI. $n = 5$. For **c**, Kaplan–Meier survival analysis. For **f–k**, $n = 5$, statistical significance was analysed by two-way ANOVA (Bonferroni). $*P < 0.05$. Error bar, means \pm SD. Data are shown from one representative experiment, based on at least three experiments, which produced similar results.

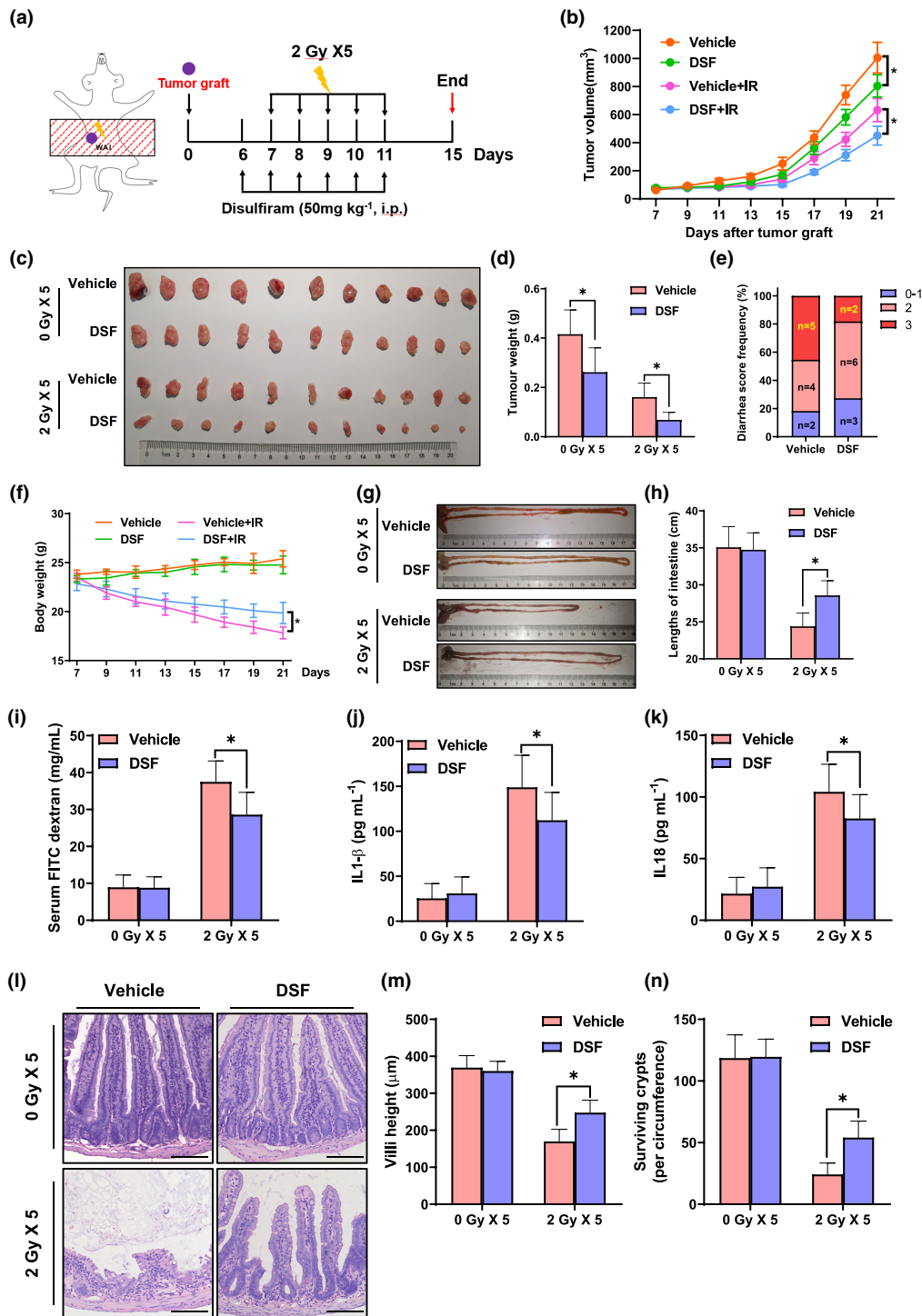


Figure 8. DSF mitigates intestinal radiotoxicity and improves radiotherapy efficacy. **(a)** Schematic diagram of DSF, tumor graft and fractionated WAI (2 Gy per fraction). **(b)** Growth curves of tumor grafts. $n = 11$. The dissected tumor grafts were photographed **(c)** and weighed **(d)** at the endpoint. $n = 11$. **(e)** The percentage of different grades of diarrhoea among mice in different groups after WAI. **(f)** The body weight of mice over time. $n = 11$. Photographs **(g)** and statistical analysis **(h)** of the intestine length of mice at the endpoint. $n = 11$. **(i)** The serum FITC-dextran level at the endpoint. $n = 11$. The IL-1 β **(j)** and IL-18 **(k)** levels in the PLF at the endpoint. $n = 11$. **(l)** H&E-stained sections of the mice intestine at the endpoint. Scale bars: 100 μm . Statistical analysis of villi height **(m)** and surviving crypts **(n)** per section at the endpoint. $n = 10$. Statistical significance was analysed by two-way ANOVA (Bonferroni). $*P < 0.05$. Error bar, means \pm SD. Data are shown from one representative experiment, based on at least three experiments, which produced similar results.

secretion of IL-1 β and IL-18 in mice, blocking of which reduces radiation-induced intestinal injury, suggesting that IL-1 β and IL-18 are important drivers of intestinal radiotoxicity. Previous studies showed that IL-1 β and IL-18 play an important role in multiple types of mucositis^{57–60} and our results are consistent with these findings, suggesting that IL-1 β and IL-18 might serve as important therapeutic targets for complications after chemoradiotherapy. In addition, the gut microbiota has been reported to regulate the secretion of IL-1 β and contribute to intestinal mucositis.^{11,37,61} Here, our results show that significant secretion of IL-1 β and IL-18 is still detected after microbiota deletion, suggesting that host-derived immunogens also account for the secretion of IL-1 β and IL-18.

In addition to the inflammatory and autoimmune diseases,^{32,62,63} self-dsDNA is an important immunogenic molecule during radiotherapy,²⁷ but whether the self-dsDNA triggers uncontrolled inflammatory intestinal toxicity is largely ignored. Recently, several studies show that radiation-induced DNA damage triggers AIM2 inflammasome-dependent pyroptosis in the nuclei of epithelial cells,^{10,27} suggesting that self-dsDNA might serve as a potential immunogen for the radiation-induced intestinal mucosa inflammation. Here, our results show that a higher level of dsDNA is positively correlated with the IL-1 β and IL-18 secretion and diarrhoea in CRC patients. A previous study showed that DNase inhibition could reduce early apoptosis of intestinal cells after radiation. Interestingly, our and another study showed that DNase could alleviate radiation-induced tissue injury and bystander effects by decreasing inflammation, indicating that the role of DNase in radiation injury needs further research. Besides, we show that radiation induces a dose-dependent release of dsDNA from the IECs, and the released dsDNA could transfer into the macrophages and trigger AIM2 inflammasome-dependent IL-1 β and IL-18 secretion in the macrophages. Unexpectedly, the purified dsDNA is difficult to activate the inflammasome in macrophages, while the HMGB1 addition rescued the pro-inflammatory effects of dsDNA, suggesting that the released dsDNA stimulates macrophages in an HMGB1-dependent manner. Further investigations indicate that the RAGE inhibitor abolished the pro-inflammatory effects of dsDNA and mitigated intestinal radiotoxicity, suggesting that dsDNA transfers into the macrophages

through the HMGB1-RAGE axis. Some pieces of evidence also suggested that HMGB1 promotes autoimmune diseases by increasing intracellular accumulation of self-dsDNA in macrophages.³² Here, our results indicate that HMGB1-RAGE plays an important role in the transfer of dsDNA into the macrophages and the subsequent inflammasome activation. Many of the previous studies focussed on the independent biological functions of the DAMP; however, our and other studies revealed the possible interactions between DAMPs and could synergistically promote tissue injury.^{64,65} Thus, the potential interactions between the DAMPs and their roles in radiation injury deserve further study.

Inflammasome has received increasing attention because of its pivotal role in multiple pathophysiological processes, including chemotherapy or radiotherapy-induced tissue injury.^{25,26,31,66–68} Our results indicate host-derived dsDNA is also involved in intestinal mucositis, broadening the understanding of inflammasome on the radiation-induced intestinal injury. In addition to a mechanistic insight into radiation-induced intestinal injury, this study also provides a potential radiotherapy adjuvant agent for further clinical evaluation. Here, our results further indicate that the FDA-approved DSF, a newly identified inflammasome inhibitor,⁵¹ has the potential to mitigate intestinal radiotoxicity and simultaneously preserve the antitumor efficacy during radiotherapy. Considering the clinical accessibility and safety, DSF may be translated into further clinical trials in the near future.

CONCLUSION

The released dsDNA from the irradiated IECs is a contributed immunogen for intestinal mucositis, and blunting the dsDNA-triggered inflammasome in macrophages may represent an exciting therapeutic strategy for intestinal radiotoxicity, while the FDA-approved DSF is a promising candidate drug for inflammasome control during abdominal radiotherapy (Figure 9).

METHODS

Reagents and resources

Detailed reagents and resources are shown in Supplementary table 1.

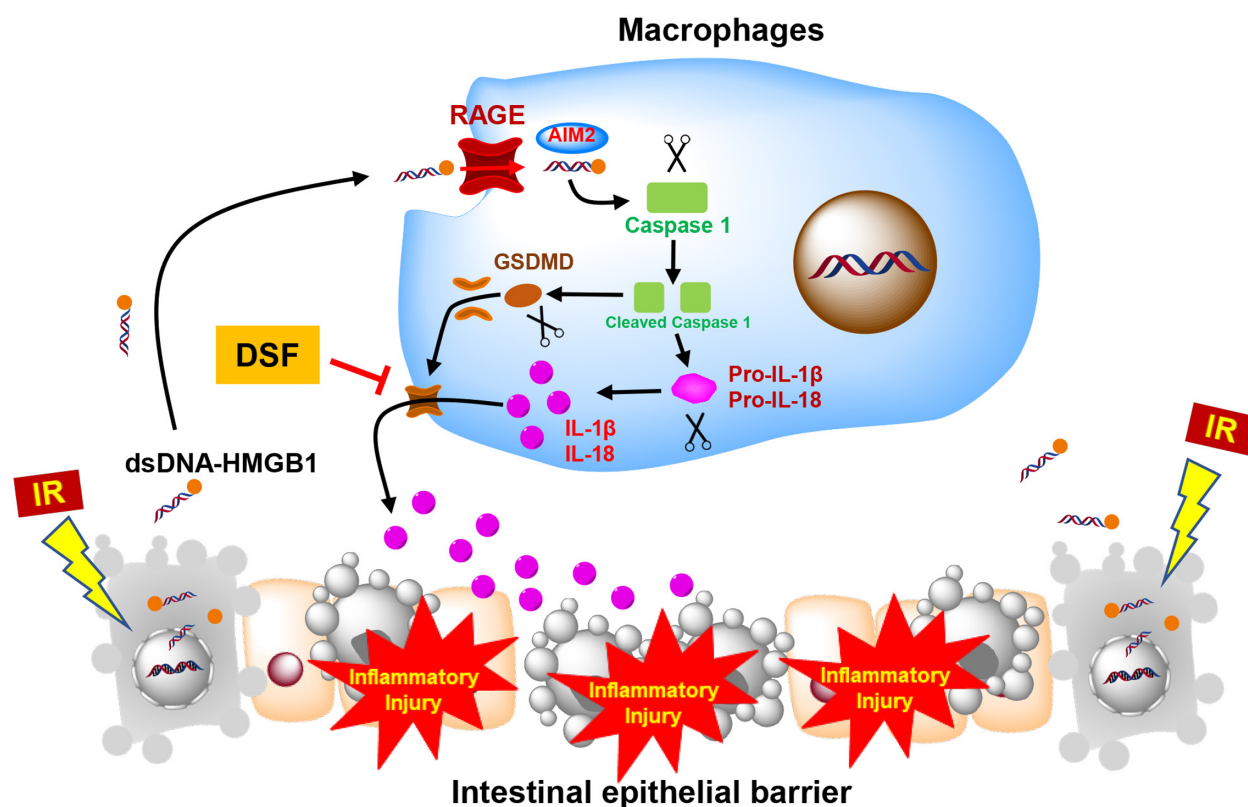


Figure 9. Targeting dsDNA-triggered AIM2 inflammasome by DSF mitigates intestinal radiotoxicity. Radiation-induced dsDNA release from the intestinal epithelial cells transfers into macrophages via the HMGB1/RAGE axis and triggers AIM2 inflammasome and the downstream consequences including pro-inflammatory cytokines secretion, which contributes to intestinal radiotoxicity. The FDA-approved DSF inhibits the secretion of pro-inflammatory cytokines and mitigates intestinal radiotoxicity by blocking the GSDMD pore formation.

Patients

Patients with CRC who attended Chengdu Military General Hospital were included with approval from the Institutional Review Board and informed consent from patients. The peripheral blood was collected before and 48 h after abdominal radiotherapy. The diarrhoea was graded according to the Common Terminology Criteria for Adverse Events (CTCAE) version 5.0. This study was approved by the Ethics Committee of Chengdu Military General Hospital (2021EC1-16).

Animals

Six- to eight-week-old male mice were purchased from the Laboratory Animal Center of the Army Medical University (AMU) and were maintained on an *ad libitum* diet. All animal experiments were approved by the Animal Care and Use Committee of the AMU.

Cell culture

The human colorectal adenocarcinoma cell line HCT116 (RRID: CVCL_0291) and mouse fibroblasts L929 (RRID:

CVCL_0462) were purchased from the American Type Culture Collection (ATCC).⁶⁹ BMMs were isolated from mouse bone marrow. All cell experiments were confirmed to be free of mycoplasma.

Drug treatment

For mice, DNase I (1 U mouse⁻¹), glycyrrhizin (10 mg kg⁻¹), disulfiram (50 mg kg⁻¹), thalidomide (25 mg kg⁻¹), belnacasan (VX-765, 25 mg kg⁻¹), dimethyl fumarate (DMF, 50 mg kg⁻¹) or vehicle (10% DMSO +90% hydrogenated castor oil) was given intraperitoneally for six consecutive days from 1 day before radiation. For cells, glycyrrhizin (1 mM), FPS-ZM1 (500 nM), rHMGB1 (10 ng mL⁻¹), DNase (0.005 U mL⁻¹) and MCC950 (10 μM) were added in the coculture media until the analysis was performed.

Diarrhoea score of mice

Diarrhoea of mice was scored 3.5 days after radiation according to the faeces as previously reported. Normal (0), slightly wet and soft stool (1), wet and unformed stool with perianal staining of the coat (2) and watery stool with perianal staining of the coat (3).

Radiation

Mice were exposed to a dose of radiation under anaesthesia using an X-RAD 160–225 instrument (Precision X-Ray, Branford, CT; filter: 2 mm Al; 50 cm, 300 kV s⁻¹, 4 mA, 0.9 Gy min⁻¹). The whole abdomen of the mice was exposed to radiation with lead shielding, and the other parts of the mouse were shielded. The total body of the mice in the control group was shielded with lead shielding before radiation exposure. Cells were exposed to the indicated dose of radiation or shielded with lead shielding.

Death determination of mice

Mice with the ruffled coat, hunched posture, unwillingness to move and 25% loss of initial body weight were identified as dead and euthanised.⁷⁰

Measurement of intestinal epithelial integrity

Epithelial integrity was evaluated by FITC-dextran assay. Mice were gavaged with 0.6 mg g⁻¹ FITC-dextran 3.5 days after radiation and sacrificed 4 h later. The serum was collected and diluted 1:1 with PBS, the fluorescence was detected using a spectrophotometer at 485/530 nm, and a standard curve was constructed through gradient dilution of FITC-dextran to quantitate FITC-dextran in the serum.

Detection of dsDNA

Peritoneal lavage fluid from mice was obtained with 1 mL PBS. Fluid and cell culture supernatants were centrifuged at 5000 rpm for 5 min twice to deplete cells, and the supernatant was then harvested. The serum from the whole blood of patients was collected before and 48 h after radiotherapy and then stored at -80°C. The PicoGreen dsDNA assay kit was used to quantitate the dsDNA in the samples by a standard curve method according to the manufacturer's instructions.

Gut microbiota depletion

As previously described, mice were treated with indicated drinking water with a combination of antibiotics, including ampicillin sodium salt (1 g L⁻¹), metronidazole (1 g L⁻¹), vancomycin hydrochloride (0.5 g L⁻¹) and neomycin (1 g L⁻¹) or vehicle for 2 weeks. Then, the DNA was extracted from the faeces of the mice using the phenol–chloroform–ethanol method, and 16S rDNA was analysed by qPCR using specific primers (Supplementary table 1) to verify the depletion efficiency.

Cytokine measurements

Cytokines including IL1-β and IL-18 were detected by ELISA kit according to the manufacturers' instructions.

HMGB1 detection

HMGB1 level was analysed by ELISA kit according to the manufacturers' instructions.

Caspase 1 activity assay

Relative Caspase 1 activity in cell lysates was detected using the Caspase 1 Assay Kit according to the manufacturers' instructions.

dsDNA purification

The purified dsDNA was extracted from the supernatant of HCT116 cells 48 h after 12 Gy radiation using phenol/chloroform/isoamyl alcohol.

BMMs culture

As reported,⁷¹ the bone marrow cells were harvested from the adult female C57BL/6 mouse, then cultured with Dulbecco's modified Eagle's medium (DMEM) supplemented with 10% foetal bovine serum (FBS) and 20% culture supernatants of L929 cells, and the culture medium was changed every 3 days. A week later, the cells (BMMs) were harvested for further experiments.

Transfection of siRNA

As previously reported,⁷² AIM2 in BMMs was knocked down using 50 nM AIM2 siRNA (5'-ACAUAGACACUGAGGGUAU-3) or negative control (5'-AAUUCUCCGACGUGUCACGU-3) with the help of Lipofectamine RNAiMAX Transfection Reagent. After 48 h, the knockdown efficiency was detected by Western blot.

Pyroptosis analysis

As previously reported,²⁷ pyroptosis was assayed by caspase-1 and propidium iodide (PI), and double-positive cells were defined as pyroptotic cells. According to the manufacturer's instructions, 5× FLICA stock solution was prepared by solubilising FLICA in 50 μL DMSO, and 1× FLICA working solution was diluted by stock solution with PBS. The samples were incubated with 1× FLICA working solution (sample: FLICA = 29:1) for approximately 1 h in the dark, then washed with PBS 1× Apoptosis Wash Buffer for three times and incubated with 3 μL PI (0.5% v v⁻¹) for 10 min. After staining, samples were analysed through flow cytometry.

LDH release detection

Lactate dehydrogenase activity was detected using the Cytotoxicity LDH Assay Kit according to the manufacturer's protocols, and LDH release was evaluated by the percentage of the LDH activity in the culture supernatant of the total lysed cells.

Histology

The mice were euthanised, and the intestine was dissected and washed in cold PBS and then fixed in 10% neutral-buffered formalin overnight. Next, samples were dehydrated with a concentration gradient of alcohol and then embedded in paraffin. Sections of tissues (5 μm) were prepared for haematoxylin and eosin (H&E) staining. Routine H&E staining was performed, and then images were captured using a light microscope.

Determination of villi height and surviving crypt

Villi height and surviving crypts were objectively quantified through intestinal images of H&E staining from at least three mice per group using ImageJ 1.37 (ImageJ, RRID: SCR_003070). The villi height was defined as the distance from the crypt villi junction to the villi tip, and the surviving crypts were defined as containing five or more adjacent chromophilic non-Paneth cells, at least one Paneth cell, and a lumen.

Immunofluorescence

Bone marrow-derived macrophages were cultured on glass coverslips. After indicated treatments, cells were fixed with 4% Neutral paraformaldehyde (15 min), permeabilised with 0.1% Triton X-100 (15 min) and blocked with 1% BSA (60 min) and then incubated with the ASC, NLRP3 or/and AIM2 antibody (1:200) overnight at 4°C. After incubation with the fluorescein-coupled secondary antibodies for 30 min, the nuclei were stained with DAPI, and then the images were captured using confocal microscopy.

Quantitative real-time PCR (qPCR) analysis

Total RNA was extracted using PureLink® RNA Mini Kit. cDNA synthesis was completed using the RevertAid First Strand cDNA Synthesis Kit, and qPCR was performed with the SYBR Green qPCR master mix according to the manufacturer's instructions. The primers are listed in Supplementary table 2. For relative quantification, data were normalised to the control using β -actin as the internal control by the ΔCT method.

Western blot

Cells were lysed in ice-cold RIPA buffer supplemented with protease inhibitors and phosphatase inhibitors, sonicated for 15 s to reduce sample viscosity and then centrifuged at $16\,000 \times g$ for 15 min at 4°C to harvest the total protein lysates. BCA method was used to determine the concentrations of the sample. Then, the samples were boiled with $1 \times$ loading buffer to 98–100°C for 10 min. 30 μg proteins from each sample were subjected to SDS-PAGE for electrophoresis and then transferred to a PVDF membrane. The membranes were blocked, incubated with primary antibodies overnight at 4°C and then incubated

with appropriate secondary antibodies for 1 h at room temperature. Tris-buffered saline with Tween (TBST) buffer was used to wash the membranes before and after incubations. The band intensity of every sample was visualised and captured using an enhanced chemiluminescence detection system (Bio-Rad Laboratories) by an ECL kit. β -Actin was used as the loading control.

Co-immunoprecipitation assay

Cell lysate containing 500 μg protein was incubated with 2 μg of indicated antibody or IgG control with rotation at 4°C overnight. Then, the immunoprecipitated complexes were combined with Protein A/G magnetic Beads and separated using eluent; finally, the samples were analysed through Western blotting.

Xenotransplantation assays

Six- to eight-week-old male BALB/c mice were from Huafukang Bioscience (Beijing, China). A total of 2×10^6 CT26 cells in PBS were subcutaneously injected at the abdominal flank region of the mice. Then, the mice were randomly divided into four groups and treated with disulfiram (50 mg kg^{-1} , i.p.) or vehicle for six consecutive days from 1 day before fractionated radiotherapy. Fractionated WAI (2 Gy per fraction) was performed daily for five consecutive days in total. The health status of the mice was observed daily, including diarrhoea score after radiation. The tumor size and bodyweight of mice were measured every 2 days, and the volume was estimated using the formula: volume = length \times width² \times 0.5. At the endpoint, the xenografts were photographed and weighed. During the radiotherapy, mice were euthanised if tumor size reached 1000 mm^3 .

Statistical analyses

Equalisation, randomisation and blinding for each group were involved in all experiments. Data are presented as means \pm standard deviations. The data were analysed in Prism 7 (RRID: SCR_002798). Statistical analysis methods were available in the corresponding figure captions. In all cases, $P < 0.05$ was considered statistically significant; ns, no significance; *, $P < 0.05$.

ACKNOWLEDGMENTS

This work was supported by the National Key Research and Development Program (2016YFC1000805); the Key Program of National Natural Science Foundation of China (82030056); and the Intramural Research Project Grants (AWS17J007 and 2018-JCJQ-ZQ-001).

AUTHOR CONTRIBUTIONS

Long Chen: Data curation; writing – original draft; writing – review and editing. **Ziwen Wang:** Conceptualization; data curation; formal analysis. **Jie Wu:** Conceptualization; data

curation; formal analysis. **Quan Yao**: Conceptualization; data curation; formal analysis. **Jingjing Peng**: Conceptualization; data curation. **Chi Zhang**: Conceptualization; data curation; formal analysis. **Hongdan Chen**: Data curation; formal analysis. **Yingjie Li**: Conceptualization. **Zhongyong Jiang**: Conceptualization. **Yunsheng Liu**: Conceptualization. **Chunmeng Shi**: Conceptualization; funding acquisition.

CONFLICT OF INTEREST

The authors declare no conflict of interest.

ETHICS APPROVAL AND CONSENT TO PARTICIPANTS

The animal experiments were approved by the Ethics Committee of the Animal Center of the Army Medical University and were carried out in accordance with the European Committee Council Directive (2010-63-EU). The experiments on human-derived blood samples were informed consent from patients, approved by the Ethics Committee of Chengdu Military General Hospital, and in accordance with the 1964 Helsinki Declaration and its later amendments or comparable ethical standards.

DATA AVAILABILITY STATEMENT

The authors declare that all data supporting the findings of this study are available within the paper and the Supporting Information and from the authors on request.

REFERENCES

- Siegel RL, Miller KD, Jemal A. Cancer statistics, 2020. *CA Cancer J Clin* 2020; **70**: 7–30.
- Miller KD, Nogueira L, Mariotto AB et al. Cancer treatment and survivorship statistics, 2019. *CA Cancer J Clin* 2019; **69**: 363–385.
- De Ruyscher D, Niedermann G, Burnet NG, Siva S, Lee AWM, Hegi-Johnson F. Radiotherapy toxicity. *Nat Rev Dis Primers* 2019; **5**: 13.
- Hauer-Jensen M, Denham JW, Andreyev HJ. Radiation enteropathy—pathogenesis, treatment and prevention. *Nat Rev Gastroenterol Hepatol* 2014; **11**: 470–479.
- Chen L, Liao F, Jiang Z et al. Metformin mitigates gastrointestinal radiotoxicity and radiosensitises P53 mutation colorectal tumours via optimising autophagy. *Br J Pharmacol* 2020; **177**: 3991–4006.
- Chater C, Saudemont A, Zerbib P. Chronic radiation enteritis. *J Visc Surg* 2019; **156**: 175–176.
- Paris F, Fuks Z, Kang A et al. Endothelial apoptosis as the primary lesion initiating intestinal radiation damage in mice. *Science* 2001; **293**: 293–297.
- Kirsch DG, Santiago PM, di Tomaso E et al. p53 controls radiation-induced gastrointestinal syndrome in mice independent of apoptosis. *Science* 2010; **327**: 593–596.
- Thermozier S, Hou W, Zhang X et al. Anti-ferroptosis drug enhances total-body irradiation mitigation by drugs that block apoptosis and necroptosis. *Radiat Res* 2020; **193**: 435–450.
- Hu B, Jin C, Li HB et al. The DNA-sensing AIM2 inflammasome controls radiation-induced cell death and tissue injury. *Science* 2016; **354**: 765–768.
- Gerassy-Vainberg S, Blatt A, Danin-Poleg Y et al. Radiation induces proinflammatory dysbiosis: transmission of inflammatory susceptibility by host cytokine induction. *Gut* 2018; **67**: 97–107.
- Indaram AV, Visvalingam V, Locke M, Bank S. Mucosal cytokine production in radiation-induced proctosigmoiditis compared with inflammatory bowel disease. *Am J Gastroenterol* 2000; **95**: 1221–1225.
- Symon Z, Goldshmidt Y, Picard O et al. A murine model for the study of molecular pathogenesis of radiation proctitis. *Int J Radiat Oncol Biol Phys* 2010; **76**: 242–250.
- Molla M, Panes J. Radiation-induced intestinal inflammation. *World J Gastroenterol* 2007; **13**: 3043–3046.
- Thomsen M, Vitetta L. Adjunctive treatments for the prevention of chemotherapy- and radiotherapy-induced mucositis. *Integr Cancer Ther* 2018; **17**: 1027–1047.
- Ryzhakov G, West NR, Franchini F et al. Alpha kinase 1 controls intestinal inflammation by suppressing the IL-12/Th1 axis. *Nat Commun* 2018; **9**: 3797.
- Tian T, Zhao Y, Yang Y et al. The protective role of short-chain fatty acids acting as signal molecules in chemotherapy- or radiation-induced intestinal inflammation. *Am J Cancer Res* 2020; **10**: 3508–3531.
- Li X, Cui W, Hull L, Wang L, Yu T, Xiao M. IL-18 binding protein (IL-18BP) as a novel radiation countermeasure after radiation exposure in mice. *Sci Rep* 2020; **10**: 18674.
- Eriguchi Y, Nakamura K, Yokoi Y et al. Essential role of IFN- γ in T cell-associated intestinal inflammation. *JCI Insight* 2018; **3**: e121886.
- Kiang JG, Smith JT, Cannon G et al. Ghrelin, a novel therapy, corrects cytokine and NF-kappaB-AKT-MAPK network and mitigates intestinal injury induced by combined radiation and skin-wound trauma. *Cell Biosci* 2020; **10**: 63.
- Hu L, Chen H, Zhang X, Feng Z, Zhang H, Meng Q. Rosiglitazone ameliorates radiation-induced intestinal inflammation in rats by inhibiting NLRP3 inflammasome and TNF- α production. *J Radiat Res* 2020; **61**: 842–850.
- Zhang C, Chen K, Wang J et al. Protective effects of crocetin against radiation-induced injury in intestinal epithelial cells. *Biomed Res Int* 2020; **2020**: 2906053.
- Zhang XM, Hu X, Ou JY et al. Glycyrrhizin ameliorates radiation enteritis in mice accompanied by the regulation of the HMGB1/TLR4 pathway. *Evid Based Complement Alternat Med* 2020; **2020**: 8653783.
- Barker CA, Kim SK, Budhu S, Matsoukas K, Daniyan AF, D'Angelo SP. Cytokine release syndrome after radiation therapy: case report and review of the literature. *J Immunother Cancer* 2018; **6**: 1.
- Man SM. Inflammasomes in the gastrointestinal tract: infection, cancer and gut microbiota homeostasis. *Nat Rev Gastroenterol Hepatol* 2018; **15**: 721–737.
- Lian Q, Xu J, Yan S et al. Chemotherapy-induced intestinal inflammatory responses are mediated by exosome secretion of double-strand DNA via AIM2 inflammasome activation. *Cell Res* 2017; **27**: 784–800.

27. Gao J, Peng S, Shan X et al. Inhibition of AIM2 inflammasome-mediated pyroptosis by Andrographolide contributes to amelioration of radiation-induced lung inflammation and fibrosis. *Cell Death Dis* 2019; **10**: 957.
28. Wu T, Liu W, Fan T et al. 5-Androstenediol prevents radiation injury in mice by promoting NF-kappaB signaling and inhibiting AIM2 inflammasome activation. *Biomed Pharmacother* 2020; **121**: 109597.
29. Vakrakou AG, Boiu S, Ziakas PD, Xingi E, Boleti H, Manoussakis MN. Systemic activation of NLRP3 inflammasome in patients with severe primary Sjogren's syndrome fueled by inflammagenic DNA accumulations. *J Autoimmun* 2018; **91**: 23–33.
30. Gaidt MM, Ebert TS, Chauhan D et al. The DNA inflammasome in human myeloid cells is initiated by a STING-cell death program upstream of NLRP3. *Cell* 2017; **171**: 1110–1124 e1118.
31. Lammert CR, Frost EL, Bellinger CE et al. AIM2 inflammasome surveillance of DNA damage shapes neurodevelopment. *Nature* 2020; **580**: 647–652.
32. Li X, Yue Y, Zhu Y, Xiong S. Extracellular, but not intracellular HMGB1, facilitates self-DNA induced macrophage activation via promoting DNA accumulation in endosomes and contributes to the pathogenesis of lupus nephritis. *Mol Immunol* 2015; **65**: 177–188.
33. Komada T, Chung H, Lau A et al. Macrophage uptake of necrotic cell DNA activates the AIM2 inflammasome to regulate a proinflammatory phenotype in CKD. *J Am Soc Nephrol* 2018; **29**: 1165–1181.
34. Morales AJ, Carrero JA, Hung PJ et al. A type I IFN-dependent DNA damage response regulates the genetic program and inflammasome activation in macrophages. *Elife* 2017; **6**: e24655.
35. Reis Ferreira M, Andreyev HJN, Mohammed K et al. Microbiota- and radiotherapy-induced gastrointestinal side-effects (MARS) study: a large pilot study of the microbiome in acute and late-radiation enteropathy. *Clin Cancer Res* 2019; **25**: 6487–6500.
36. Sokol H, Adolph TE. The microbiota: an underestimated actor in radiation-induced lesions? *Gut* 2018; **67**: 1–2.
37. Xiao HW, Cui M, Li Y et al. Gut microbiota-derived indole 3-propionic acid protects against radiation toxicity via retaining acyl-CoA-binding protein. *Microbiome* 2020; **8**: 69.
38. Cui M, Xiao H, Li Y et al. Sexual dimorphism of gut microbiota dictates therapeutics efficacy of radiation injuries. *Adv Sci (Weinh)* 2019; **6**: 1901048.
39. Ferreira MR, Muls A, Dearnaley DP, Andreyev HJ. Microbiota and radiation-induced bowel toxicity: lessons from inflammatory bowel disease for the radiation oncologist. *Lancet Oncol* 2014; **15**: e139–e147.
40. Rostami A, Lambie M, Yu CW, Stambolic V, Waldron JN, Bratman SV. Senescence, necrosis, and apoptosis govern circulating cell-free DNA release kinetics. *Cell Rep* 2020; **31**: 107830.
41. de Jong PR, Takahashi N, Harris AR et al. Ion channel TRPV1-dependent activation of PTP1B suppresses EGFR-associated intestinal tumorigenesis. *J Clin Invest* 2014; **124**: 3793–3806.
42. Yang S, Wang B, Humphries F et al. Pellino3 ubiquitinates RIP2 and mediates Nod2-induced signaling and protective effects in colitis. *Nat Immunol* 2013; **14**: 927–936.
43. Ashrafizadeh M, Farhood B, Elejojo Musa A, Taeb S, Najafi M. Damage-associated molecular patterns in tumor radiotherapy. *Int Immunopharmacol* 2020; **86**: 106761.
44. Hornung V, Ablasser A, Charrel-Dennis M et al. AIM2 recognizes cytosolic dsDNA and forms a caspase-1-activating inflammasome with ASC. *Nature* 2009; **458**: 514–518.
45. Morrone SR, Matyszewski M, Yu X, Delannoy M, Egelman EH, Sohn J. Assembly-driven activation of the AIM2 foreign-dsDNA sensor provides a polymerization template for downstream ASC. *Nat Commun* 2015; **6**: 7827.
46. Hu S, Peng L, Kwak YT et al. The DNA sensor AIM2 maintains intestinal homeostasis via regulation of epithelial antimicrobial host defense. *Cell Rep* 2015; **13**: 1922–1936.
47. Zhong Z, Liang S, Sanchez-Lopez E et al. New mitochondrial DNA synthesis enables NLRP3 inflammasome activation. *Nature* 2018; **560**: 198–203.
48. Shimada K, Crother TR, Karlin J et al. Oxidized mitochondrial DNA activates the NLRP3 inflammasome during apoptosis. *Immunity* 2012; **36**: 401–414.
49. Tapia-Abellan A, Angosto-Bazarra D, Martinez-Banaclocha H et al. MCC950 closes the active conformation of NLRP3 to an inactive state. *Nat Chem Biol* 2019; **15**: 560–564.
50. Stack JH, Beaumont K, Larsen PD et al. IL-converting enzyme/caspase-1 inhibitor VX-765 blocks the hypersensitive response to an inflammatory stimulus in monocytes from familial cold autoinflammatory syndrome patients. *J Immunol* 2005; **175**: 2630–2634.
51. Hu JJ, Liu X, Xia S et al. FDA-approved disulfiram inhibits pyroptosis by blocking gasdermin D pore formation. *Nat Immunol* 2020; **21**: 736–745.
52. Humphries F, Shmuel-Galia L, Ketelut-Carneiro N et al. Succination inactivates gasdermin D and blocks pyroptosis. *Science* 2020; **369**: 1633–1637.
53. Skrott Z, Mistrik M, Andersen KK et al. Alcohol-abuse drug disulfiram targets cancer via p97 segregase adaptor NPL4. *Nature* 2017; **552**: 194–199.
54. Terashima Y, Toda E, Itakura M et al. Targeting FROUNT with disulfiram suppresses macrophage accumulation and its tumor-promoting properties. *Nat Commun* 2020; **11**: 609.
55. Wu W, Yu L, Pu Y, Yao H, Chen Y, Shi J. Copper-enriched prussian blue nanomedicine for in situ disulfiram toxicification and photothermal antitumor amplification. *Adv Mater* 2020; **32**: e2000542.
56. Choi SA, Choi JW, Wang KC et al. Disulfiram modulates stemness and metabolism of brain tumor initiating cells in atypical teratoid/rhabdoid tumors. *Neuro Oncol* 2015; **17**: 810–821.
57. Lima-Junior RC, Freitas HC, Wong DV et al. Targeted inhibition of IL-18 attenuates irinotecan-induced intestinal mucositis in mice. *Br J Pharmacol* 2014; **171**: 2335–2350.
58. Kanarek N, Grivnennikov SI, Leshets M et al. Critical role for IL-1 β in DNA damage-induced mucositis. *Proc Natl Acad Sci USA* 2014; **111**: e702–e711.
59. de Mooij CEM, Netea MG, van der Velden W, Blijlevens NMA. Targeting the interleukin-1 pathway in patients with hematological disorders. *Blood* 2017; **129**: 3155–3164.

60. Arifa RD, Madeira MF, de Paula TP *et al.* Inflammasome activation is reactive oxygen species dependent and mediates irinotecan-induced mucositis through IL-1 β and IL-18 in mice. *Am J Pathol* 2014; **184**: 2023–2034.
61. Guo H, Chou WC, Lai Y *et al.* Multi-omics analyses of radiation survivors identify radioprotective microbes and metabolites. *Science* 2020; **370**: eaay9097.
62. Lou H, Pickering MC. Extracellular DNA and autoimmune diseases. *Cell Mol Immunol* 2018; **15**: 746–755.
63. Benmerzoug S, Ryffel B, Togbe D, Quesniaux VFJ. Self-DNA sensing in lung inflammatory diseases. *Trends Immunol* 2019; **40**: 719–734.
64. Liu L, Yang M, Kang R *et al.* HMGB1-DNA complex-induced autophagy limits AIM2 inflammasome activation through RAGE. *Biochem Biophys Res Commun* 2014; **450**: 851–856.
65. Liaw PC, Ito T, Iba T, Thachil J, Zeerleder S. DAMP and DIC: the role of extracellular DNA and DNA-binding proteins in the pathogenesis of DIC. *Blood Rev* 2016; **30**: 257–261.
66. Karki R, Kanneganti TD. Diverging inflammasome signals in tumorigenesis and potential targeting. *Nat Rev Cancer* 2019; **19**: 197–214.
67. Wu C, Lu W, Zhang Y *et al.* Inflammasome activation triggers blood clotting and host death through pyroptosis. *Immunity* 2019; **50**: 1401–1411 e1404.
68. Samir P, Kesavardhana S, Patmore DM *et al.* DDX3X acts as a live-or-die checkpoint in stressed cells by regulating NLRP3 inflammasome. *Nature* 2019; **573**: 590–594.
69. Huang Y, Zhou J, Luo S *et al.* Identification of a fluorescent small-molecule enhancer for therapeutic autophagy in colorectal cancer by targeting mitochondrial protein translocase TIM44. *Gut* 2018; **67**: 307–319.
70. Wan H, Yang H, Shore DA *et al.* Structural characterization of a protective epitope spanning A (H1N1)pdm09 influenza virus neuraminidase monomers. *Nat Commun* 2015; **6**: 6114.
71. Kimura T, Nada S, Takegahara N *et al.* Polarization of M2 macrophages requires Lamtor1 that integrates cytokine and amino-acid signals. *Nat Commun* 2016; **7**: 13130.
72. Prieto P, Rosales-Mendoza CE, Terron V *et al.* Activation of autophagy in macrophages by pro-resolving lipid mediators. *Autophagy* 2015; **11**: 1729–1744.

Supporting Information

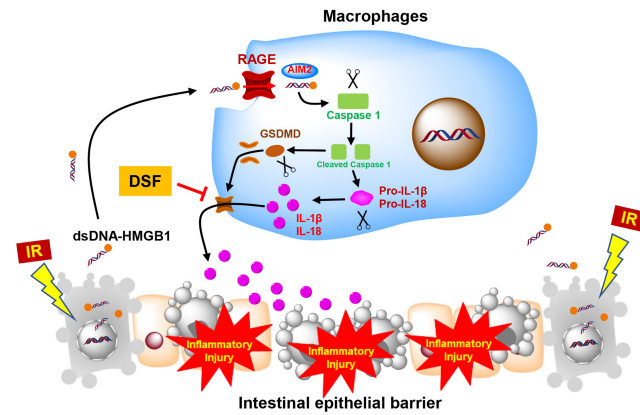
Additional supporting information may be found online in the Supporting Information section at the end of the article.



This is an open access article under the terms of the [Creative Commons Attribution-NonCommercial-NoDerivs](#) License, which permits use and distribution in any medium, provided the original work is properly cited, the use is non-commercial and no modifications or adaptations are made.

Graphical Abstract

The contents of this page will be used as part of the graphical abstract of html only. It will not be published as part of main.



In this study, we found that inflammasome-dependent IL-1 β and IL-18 secretion accounts for intestinal radiotoxicity. Our results showed that released dsDNA from the irradiated IECs transfers into macrophages and triggers AIM2 inflammasome-dependent IL-1 β and IL-18 secretion. Finally, we found that FDA-approved disulfiram is a promising candidate drug for mitigating intestinal radiotoxicity by controlling inflammasome-dependent IL-1 β and IL-18 secretion.